Solid-State Phase Transition of a Hydrated β-Cyclodextrin Dimeric Complex

Nicole Rysanek* and Michel Coquillay

Laboratoire de Physique, Faculté de Pharmacie, Université Paris-Sud, 92296 Chatenay-Malabry Cedex, France

Claudie Bourgaux

Laboratoire pour l'Utilisation du Rayonnement Electromagnétique (LURE), Université Paris-Sud, 91405 Orsay, France

Michel Ollivon

Equipe Physicochimie des Systèmes Polyphasés, UMR CNRS 8612, Université Paris-Sud, 92296 Chatenay-Malabry Cedex, France

Received: December 12, 2001; In Final Form: September 12, 2002

The thermal and structural behavior of the complex β-cyclodextrin 1,7-dioxaspiro[5,5]undecane·9H_2O is studied between 23 and 150 °C using the coupling of differential scanning calorimetry (DSC) and time-resolved X-ray diffraction as a function of temperature (XRDT). A drastic structural change between the low-temperature (LT) and the high-temperature (HT) phases, correlated with an endothermic DSC peak, shows that a solid-state phase transition takes place at about 110 °C on heating. A model for the HT phase is built from the knowledge of the LT phase crystal structure and is ascertained by simulated X-ray diffraction patterns. Both LT and HT structures are columnar, and the phase transition is explained by the loss of water molecules located between the β-cyclodextrin channels, leading to their close contact. The HT phase is a new structural form of the β-cyclodextrin complex that is fully dehydrated. The recordings of both DSC and XRDT from the same sample employed for the first time to the study of cyclodextrin phase transition allowed an unambiguous splitting of the thermal and structural evolutions and was revealed to be a very efficient tool for the monitoring of kinetically controlled processes.

Introduction

Cyclodextrins consist of macrocyclic oligosaccharides. These ring-shaped molecules are well known for their ability to form inclusion complexes with a variety of guest molecules located inside their cavities.[1−4] The β-cyclodextrin molecules (βCD) contain seven glucose units. In most cases, complexes obtained with βCD in aqueous solution crystallize in one of the following two structural types: channel or cage.[3−5] The present compound is a hydrated complex that belongs to the channel type, and the guest molecule is the main pheromone component of the olive fruit fly (1,7-dioxaspiro[5,5]undecane). Moreover, the crystal structure is stabilized by water molecules located inside the interstitial space between adjacent βCD molecules.[6]

The first aim of this study was to understand how the release process of the guest molecule can be influenced by temperature elevation. To make an experimental approach to this problem, a powder sample was submitted to regular heating, and the modifications were simultaneously examined by differential scanning calorimetry (DSC) and X-ray diffraction as a function of temperature (XRDT), which is particularly convenient to the correlation of the structural modifications with the thermal evolution. The experimental results obtained in this way show that the thermal behavior of the compound is strongly related to the dehydration mechanism. Previous studies of this phenomenon concern essentially βCD hydrate[7,8] and more recently hydrated native and methylated βCD complexes.[9,10]

This coupling of DSC with time-resolved synchrotron XRDT measurements was achieved a few years ago.[11] This method, which is easy to perform, gives relevant results about various phenomena such as dehydration. Recently, it was used to monitor the crystallization of amylose−lipid complexes during maize starch melting.[12]

Experimental Section

Materials. βCD was purchased from Wacker. Racemic 1,7-dioxaspiro[5,5]undecane (spiro) was synthesized according to the procedure given by Mori.[13] βCD was dissolved in water to obtain a saturated solution that was simultaneously stirred and heated to 50 °C. At this stage, the heating was stopped, spiro was added to the solution submitted to continuous stirring during 3 days or more, and then the flask contents were filtered on a Whatman filter with a vacuum water pump and the white precipitate was dried at ambient temperature. After grinding the complex to a fine powder, a sample of about 8 mg was loaded into a special glass capillary whose outer diameter is 1.5 mm (GLAS, Müller, Berlin, Germany) in order to perform X-ray analysis.

DSC Measurements. DSC measurements were performed on a Perkin-Elmer (DSC7) differential scanning calorimeter equipped with an Intracooler II cooling device by using PYRIS software; the sample was analyzed in sealed aluminum capsules.

* Corresponding author. E-mail: nicole.rysanek@cep.u-psud.fr. Fax: 33-(1)46835630.

10.1021/jp015607w CCC: $22.00
Published on Web 10/17/2002

Coupled DSC and XRDT measurements were performed simultaneously on the same sample contained in a glass capillary using a MICROCALIX instrument.[11] A calorimeter screen was maintained at 20 °C while less than 1 V was applied to the cooling Peltier module. Both DSC and XRDT recordings were duplicated; the data presented here result from the first analysis, the second one giving identical results within experimental errors. The heating was monitored by a temperature controller at a rate of 2 °C/min so that the temperature was linearly scanned with an accuracy of 0.1 °C over the range 23−150 °C.

XRDT−DSC Measurements. X-ray diffraction measurements were carried out using a monochromatic ($\lambda = 1.489$ Å) focused X-ray beam at station D24 (about 5 10^9 photons/s/mm^2) of the DCI synchrotron at L.U.R.E. (Orsay, France). The sample holder coupling DSC and XRDT was specially developed for the D24 bench;[11] it allows X-ray diffraction patterns to be recorded as a function of temperature during the thermal evolution, hence both structural and thermal analyses can be performed on the same sample. X-ray diffraction intensities were simultaneously recorded on a 1024 channel linear detector, and the data were stored in a PC, each frame corresponding to a time exposure of 59 s. For this study, 65 frames separated by a dead time of 1 s were collected with a heating rate of 2 °C/min over a temperature range of 23−150 °C. Then the sample was quickly cooled to 23 °C, and an additional frame was recorded. The sample−detector distance (about 300 mm) allows us to explore the region of the X-ray diffraction pattern $0 < q < 1.75$ Å^{-1} where q defines the scattering vector ($q = 4\pi \sin\theta/\lambda$ where θ is the Bragg angle and λ the X-ray wavelength). Intensity data were corrected in order to eliminate the scattering background due to the glass capillary.

Results and Discussion

General Overview. DSC measurements performed simultaneously with XRDT show the occurrence of a thermal event in the range 94−126 °C; a broad endothermic peak reaching a maximum at 117 °C is observed (Figure 1A). Preliminary DSC measurements, performed with a Perkin-Elmer DSC7 calorimeter, on a sample of the same weight and for the same heating rate give a very broad endothermic peak reaching a maximum at 67 °C (Figure 1A inset). In both cases, an endothermic peak is observed; an explanation of the differences observed in both DSC techniques is given below.

The X-ray diffraction patterns recorded as a function of temperature show a drastic structural change at about 110 °C, which is well correlated to the endothermic peak observed in the DSC curve. The discrete character of the spectra at high temperature suggests that the compound remains in the crystalline state, which indicates the existence of two different crystalline phases referred to LT and HT phases for low and high temperature, respectively (Figure 2). To define more precisely the phase transition, the evolution of the intensities of four selected peaks representative of both phases was plotted as a function of temperature: *L2* and *L7* for the LT phase and *H1* and *H2* for the HT phase (Figure 1b). In the region of the LT phase, the intensities of peaks *L2* and *L7* remain approximately constant at $T < 101$ °C, and then, after a marked decrease, they are almost vanishing at $T > 117$ °C. The opposite behavior is noticed for peaks *H1* and *H2*, which characterizes the region of HT phase at $T > 117$ °C. The phase transition lies in the range 101 °C $< T <$ 117 °C, which is well correlated with the DSC curve (Figure 1A).

These results are perfectly reproducible when the same heating rate is applied (here, 2 °C/min). Moreover, when the sample is quickly cooled to 23 °C after regular heating from 23 to 150 °C, the X-ray diffraction pattern displays the feature of the HT phase. When this sample of the HT phase is heated again to 150 °C with a heating rate 2 °C/min, no phase transition is observed either in the diffraction patterns or in the DSC measurements. These observations show that the phase transition is irreversible with respect to the temperature.

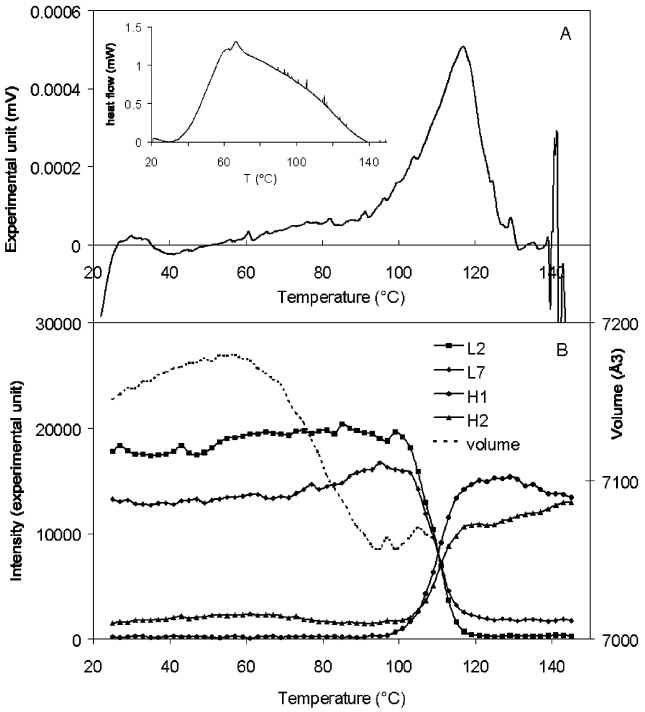

Figure 1. Characterization of the phase transition: (A) DSC recording obtained by the (DSC, XRDT) technique; inset displays the DSC curve recorded with the Perkin-Elmer apparatus; (B) evolution of maximum intensity for selected peaks versus temperature in the range 25−145 °C. The unit cell volume calculated at each temperature is also shown (- - -).

Structural Analysis of the LT Phase. The structure analysis of the LT phase was achieved a few years ago from X-ray diffraction performed on a single crystal in contact with a mother liquor at room temperature. The crystallographic data are the following: monoclinic space group, *C*2; cell parameters, $a =$ 19.368 Å, $b = 24.45$ Å, $c = 15.94$ Å, $\beta = 108.72°$; cell volume, $V = 7149$ Å^3; molecules per cell, $Z = 4$. It is a channel-type structure with guest molecules located inside the boundless continuous cavity formed by the βCD dimers stacked along the *c* axis.[6] Figure 3 displays the arrangement of channels in the crystal structure of the LT phase: both dimers B and C are directly linked to dimer A by H-bonds between hydroxyl groups, whereas they are held together through a network of H-bonded water molecules inside the interstitial space, which is also endlessly extended along the *c* axis. The asymmetric unit contains 1 molecule of βCD and 9 water molecules distributed over 16 sites, some of them being partially populated.

In the first step, the knowledge of the cell parameters was used to calibrate the experimental data, and then, the LT X-ray diffraction pattern at 23 °C was compared to the simulated X-ray diffraction pattern calculated with the known atomic coordinates by using FULPROF software.[15] Figure 4 shows that there is good agreement between both patterns so that it is possible to index the experimental data. PEAKFIT software (Jandel Scientific, Germany) was used to locate single reflections in the diffraction patterns; however, the low resolution of the spectra prevents the closest reflections from being identified.

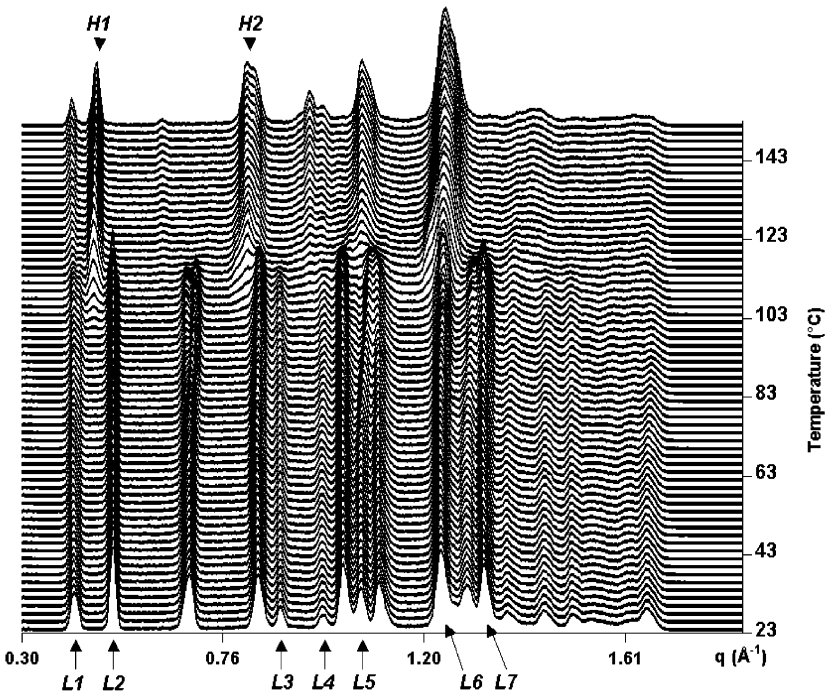

Figure 2. Three-dimensional plots of X-ray diffraction data recorded simultaneously with DSC during sample heating at 2 °C/min from 23 to 150 °C. Selected peaks *L1* to *L7* in the LT phase and *H1* and *H2* in the HT phase are used for the analysis of thermal evolution.

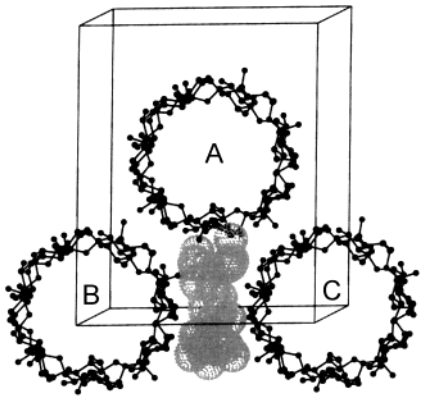

Figure 3. Ball-and-stick drawing of the LT phase packing viewed along the *c* axis (guest molecules and H-atoms are not shown); both the *a* axis (horizontal) and the *b* axis (vertical) belong to the drawing plane (SYBYL[14]). The picture results from a previous single-crystal structure analysis (interstitial water molecules are shown in CPK style).

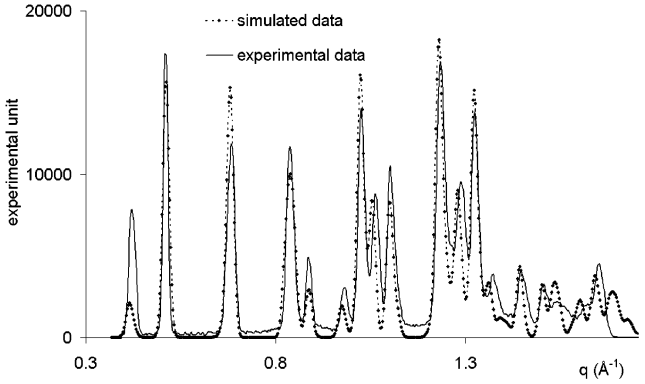

Figure 4. LT phase: comparison between the experimental diffraction diagram at 23 °C from XRDT measurements (—) and the simulated diffraction diagram calculated with the atomic coordinates given by the single-crystal structure analysis of the compound (· · ·).

Detailed examination of the LT X-ray diffraction patterns versus temperature gives some insight into the thermal behavior of the crystal structure between 23 and 110 °C. Figure 5 displays the thermal evolution of six relevant diffraction peaks that have been indexed unambiguously. By using the Bragg law for the monoclinic system, $q/2\pi = (h^2a^{*2} + k^2b^{*2} + l^2c^{*2} - 2hla^*c^* \cos\beta)^{1/2}$ where a^*, b^*, and c^* are the reciprocal parameters, b^* is easily derived from the q value of reflection (020), hence a^* and c^* can be calculated from reflections (310) and (022), respectively, and the angle β is deduced from reflection (20-2).

The evolution of the cell parameters as a function of temperature is displayed in Figure 6. An exhaustive study of the other single reflections shows that their evolution versus temperature well agrees with the previous results. For 23 °C < T < 53 °C, the slightly increasing rate of the cell parameters with temperature (0.5% maximum for volume V) is correlated to the usual thermal dilatation, for which the content of the unit cell remains unchanged. For T > 53 °C, an opposite evolution of cell parameters is observed, with a significant decrease of parameters a and sin β; the corresponding volume variation (about −1.5% at T = 100 °C) suggests that the content of the unit cell is smoothly reorganized.

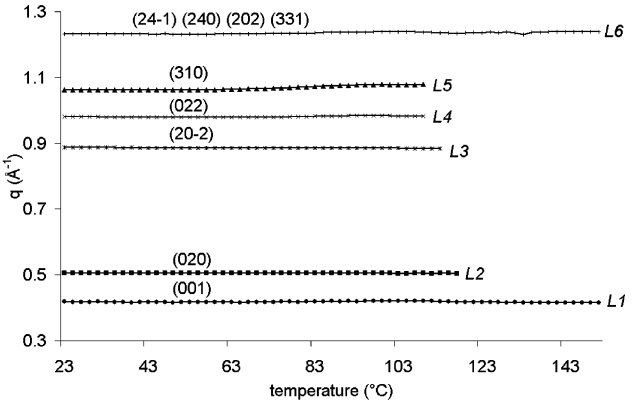

Figure 5. Thermal evolution of well-resolved diffraction peaks. The reflection indexes are related to the LT phase only. Peaks *L2* to *L5* are used to calculate the unit cell parameters.

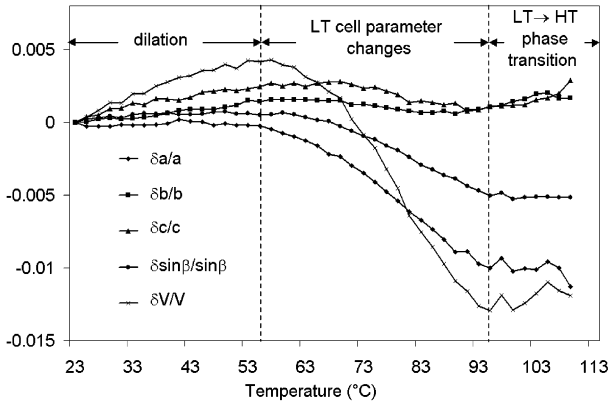

Figure 6. Thermal evolution of the unit cell parameters of the LT phase. The maximum value of ΔV between 55 and 95 °C is 126 Å^3.

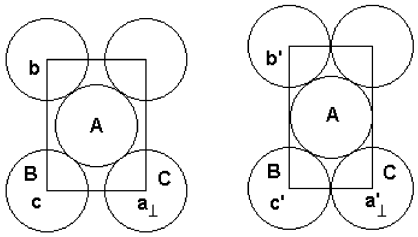

Figure 7. Schematic representation of the unit cell of the LT phase (left) and the HT phase (right); the *b* axis belongs to the drawing plane, and the *c* axis is perpendicular to it; $a_\perp$ refers to the *a*-axis projection. In the LT phase, water molecules are located in the gap between channels B and C. In the HT phase, the gap vanishes because water molecules migrate out of the crystal.

Structural Analysis of the HT Phase. X-ray patterns for HT and LT phases are quite different. It is not possible to determine directly the unit cell parameters of the HT phase because of the low resolution of powder spectra. To verify whether the crystal structure of the HT phase matches one of the four known packing modes of βCD dimeric complexes,[16] the experimental data were compared to the simulated powder spectra of known structures reported in the literature by using FULPROF. There is no similarity, and to our knowledge, the crystal structure of the HT phase has not yet been observed.

To determine which unit cell is related to the HT-phase spectra, we built a model in an intuitive way. First, we hypothesised from the outstanding constant *q* value of peak *L1* related to reflection (001) (Figure 5) that the parameter *c* remains unchanged for the whole process, including both LT and HT domain; hence, we inferred that the distortion of the unit cell can be described exclusively in the plane orthogonal to the *c* axis, as shown in Figure 7. In this drawing, the projection is face-centered because of the Bravais-type *C* unit cell, and βCD molecules appear as almost perfect circles because they are stacked along the *c* axis. In the packing of the LT phase, channels A are in close contact with channels B and C, whereas there is a gap between B and C with water molecules located inside it. We supposed that the phase transition consists of the departure of water molecules, which leads to a vanishing gap and close contact between channels B and C. Under this hypothesis, the new parameters $a \sin \beta$ and *b* can be calculated readily; nevertheless, there is a lack of information from which to determine the new value of angle β, so we have assumed this last parameter remains unchanged. Thus, the crystallographic data of the new cell should be monoclinic space group *C*2, $a = 16.12$ Å, $b = 26.44$ Å, $c = 15.95$ Å, $\beta = 108.72°$, $V = 6438$ Å^3, and $Z = 4$. Hence, it is easy to transform the atomic coordinates from the LT unit cell to those of the new cell and then to visualize the hypothetical structure on a graphical power station, as shown in Figure 8. The simulated X-ray pattern calculated using FULLPROF was compared with the HT experimental pattern (Figure 9). The good agreement between both spectra proves that this structural model is correct.

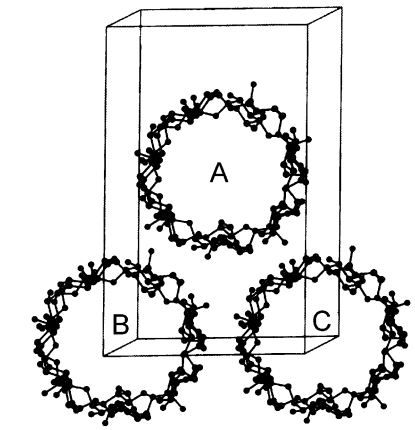

Figure 8. Ball-and-stick drawing of the HT phase packing viewed along the *c* axis (H-atoms not shown); both the *a* axis (horizontal) and the *b* axis (vertical) belong to the plane drawing (SYBYL[14]). The picture displays the structural model based on the collapse of interstitial spaces between βCD channels.

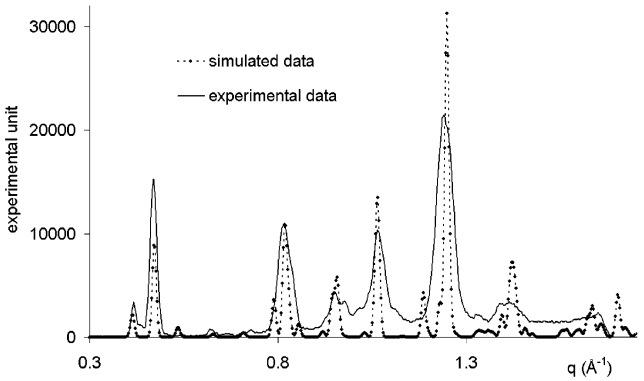

Figure 9. HT phase: comparison between the experimental diffraction diagram at 125 °C from XRDT measurements (—) and the simulated diffraction diagram calculated with the atomic coordinates of the structural hypothesis (• • •).

Furthermore, careful analysis of the XRDT patterns of Figure 2 shows that an intermediate phase is formed quickly in the range 110−123 °C with the occurrence of lines at $q = 0.79$, 1.04, and 1.21 Å^{-1}. Then, these lines vanish, and only the HT lines subsist. This fact can be interpreted either as the formation of a small amount of an additional phase that disappears at about 125 °C or as a transitory loss of symmetry of the HT phase. It was not possible to determine unambiguously which mechanism is the right one.

Hydration Number Evolution. Since the LT → HT phase transition is closely correlated to a mechanism of hydration/dehydration, precise weighing measurements have been performed on a sample of the complex at three different stages to deduce the variation of the hydration number Δn (*n* is the number of water molecules per βCD) from the mass evolution Δm. The results are listed in Table 1: stage a is referred to the freshly prepared powder at ambient atmosphere and temperature; stage b is obtained after dehydration of the sample by heating at 40 °C for 1 h; and stage c is obtained from stage b after hydration by exposing the sample to an atmosphere with 95% humidity given by a saturated aqueous solution of Na_2HPO_4. Materials in stages a, b, and c are identified by X-ray diffraction

TABLE 1: Changes in Hydration Number during Transitions

	a (LT)	*b* (HT)	*c* (LT)
m (mg)	33.8	31.4	35.4
$\Delta m/m_b$ (%)		-7.6 ($a \rightarrow b$)	$+12.7$ ($b \rightarrow c$)
Δn[a] hydration number changes		-5.5 ($a \rightarrow b$)	$+9.1$ ($b \rightarrow c$)

[a] Δn is obtained with an accuracy of $\pm 0.5 H_2O$.

to be LT, HT, and LT phases, respectively. Repeated measurements of steps (b → c) and (c → b) for the same sample give well-reproducible results.

Since the value of the hydration number (9 water molecules) is unambiguously known from X-ray diffraction on wet single crystals, the value of $\Delta n = +9.1$ for step (b → c) suggests that stage c is the fully hydrated LT phase, and the value of $\Delta n = -5.5$ for step (a → b) shows that stage a is the LT phase that is not water saturated. These results indicate that the HT phase is derived, even at low temperature, from the LT phase by the loss of all interstitial water molecules and that the process is entirely reversible with respect to the humidity of the surrounding atmosphere. Another way to estimate the hydration number consists of applying the close-packing rule to the crystal structure. The unit cell volume of the HT phase is reduced by about 711 Å^3 with respect to those of the LT phase. The mean molar volume for non-H atoms in the present structure is 18.4 Å^3, which corresponds to a spherical cavity whose radius is 1.64 Å. Hence, the volume change must be attributed to a mean loss of 9.6 non-H atoms, that is to say, 9.6 water molecules, in the asymmetric unit, which is in good agreement with the value given in Table 1. Moreover, the calculation of the mean radius of accessible volume in the interstitial channels of the HT phase is about 1.2 Å, which is too small to include an oxygen atom with regard to its radius of 1.64 Å and the standard van der Waals radius of 1.54 Å given in the literature.[17] In the same way, the decreasing unit cell volume of about 126 Å^3 in the range 55−95 °C pointed out in Figure 6 corresponds to the departure of 1.7 water molecules in the asymmetric unit of the LT phase, which is not sufficient to induce the phase transition. Both approaches are in good agreement, suggesting that there is no water in the HT phase.

Interpretation of DSC Measurements. To correlate the thermal evolution to the structural changes, the plots of data collected by coupled XRDT−DSC measurements are grouped in the same Figure with an identical temperature scale (Figure 1): (A) DSC curve and (B) intensity peak analysis. The DSC curve presented in Figure 1A shows a broad endothermic peak in the range 95−126 °C, which is clearly related to the LT → HT phase transition. This one is also observed by XRDT and corresponds to an abrupt structural change (Figure 1B): the transition is observed around 110 °C and spreads from 105 to 117 °C just following a domain where there is no further change in the cell parameters. Thus, three domains from which a transition mechanism can be deduced are clearly evidenced from the comparison of Figures 1 and 6. First, the cell dilates from 25 to 55 °C, and then until 95 °C, water starts to leave the crystal structure, and the cell parameters are progressively modified by water departure. In the third step, no further parameter change is accepted by the structure, which leads to the brutal irreversible transition LT → HT.

Therefore, the process can be described by the equation

$$\beta\text{CD}, n\text{H}_2\text{O(LT)} \rightarrow \beta\text{CD(HT)} + n\text{H}_2\text{O}$$

where n is the hydration number. The associated enthalpy change ΔH must be given by the equation

$$\Delta H = \Delta H_s + \Delta H_w$$

where ΔH_s refers to the solid−solid phase transition of the material and ΔH_w, to the thermal evolution of expelled water; consequently, ΔH highly depends on the thermal history of the water. The two DSC curves obtained by the coupled XRDT−DSC technique and the DSC7 Perkin-Elmer apparatus are not similar (Figure 1A). The former is a broad peak reaching a maximum at $T = 117$ °C and giving $\Delta H = 273$ kJ mol^{-1}, whereas the later is a very broad peak with a maximum at $T = 67$ °C and $\Delta H = 410$ kJ mol^{-1}. These differences should be attributed to the influence of the cell geometry of the apparatus. In the DSC7, the sample is contained in a flat capsule, whereas in the coupled XRDT−DSC apparatus, it is contained in a capillary so that the contact areas between the powder and the ambient atmosphere are about 50 mm^2 and 1 mm^2, respectively. Consequently, the diffusion of water through the material and its vaporization is easily achieved in the DSC7 cell, which explains the lower temperature of transition and the higher value of ΔH. Conversely, the shape of the capillary gives a longer diffusion path and delays the vaporization of water, which is confirmed by the observation of water condensation in the cold area inside the capillary after the experiment's completion and its cooling.

Concluding Remarks

The LT → HT phase transition of the studied βCD complex is induced by a temperature increase and is chiefly governed by a dehydration process. The configuration of the LT phase is assumed to be unchanged for $T < 53$ °C; then, for 53 °C $< T <$ 101 °C, the heating causes some less energetically hydrogen-bonded water molecules to migrate out of the crystal. This migration is highly facilitated by the existence of diffusion paths in the direction of the c axis. The expulsion process is accelerated for $T > 101$ °C. The remaining water molecules are unable to maintain the crystal structure unchanged, which leads to a sudden collapse of the interstitial space between channels B and C. This feature exemplifies the phase transition occurring for 101 °C $< T <$ 117 °C. The crystal structure of the HT phase consists of close-packed βCD channels where interstitial water molecules must be absent.

At last, we have to consider what happens to the volatile guest during heating. Studies reported by Szetjli[18] mention that the βCD complex of volatile oil (anethum oil) is stable during heating at least up to 140 °C. DSC measurements on a hydrated βCD complex[19] show a dissociation in the range 235−270 °C. In the previous study of the crystal structure of the βCD−spiro complex, it was shown that the channel packing of the LT phase contributes to the great stability of the complex and makes the release of the guest difficult.[6] From the model proposed in the present study, it is shown that the phase transition does not alter the channel-mode packing, hence it is very probable that the guest remains trapped even at high temperature.

Acknowledgment. We gratefully thank G. Keller for the elaboration of the "Microcalix" XRDT calorimeter.

References and Notes

(1) Szejtli, J. *Cyclodextrin Technology*; Kluwer Academic Publishers: Dordrecht, The Netherlands, 1989.

(2) Szejtli, J. *Chem. Rev.* **1998**, *5*, 1743.

(3) Saenger, W.; Jacob, J.; Gessler, K.; Steiner, T.; Hoffmann, D.; Sanbe, H.; Koizumi, K.; Smith, S. M.; Takaha, T. *Chem. Rev.* **1998**, *5*, 1787.

(4) Harata, K. *Chem. Rev.* **1998**, *5*, 1803.

(5) Le Bas, G.; Rysanek, N. *Cyclodextrins and Their Industrial Uses*; Duchêne, D., Ed.; Editions de Santé: Paris, 1987; Chapter 3.

(6) Rysanek, N.; Le Bas, G.; Villain, F.; Tsoucaris, G. *Acta Crystallogr., Sect. C* **1996**, *52*, 2932.

(7) Steiner, T.; Koellner, G.; Ali, S.; Zakim, D.; Saenger, W. *Biochem. Biophys. Res. Commun*. **1992**, *188*, 1060.

(8) Steiner, T.; Koellner, G. *J. Am. Chem. Soc*. **1994**, *116*, 5122.

(9) Caira, M. R.; Bourne, S. A.; Mvula, E. *J. Therm. Anal. Calorim.* **1999**, *56*, 1329.

(10) Stezowski, J. J.; Parker, W.; Hilgenkamp, S.; Gdaniec, M. *J. Am. Chem. Soc*. **2001**, *123*, 3919.

(11) Keller, G.; Lavigne, F.; Forte, L.; Andrieux, K.; Dahim, M.; Loisel, C.; Ollivon, M.; Bourgaux, C.; Lesieur, P. *J. Therm. Anal*. **1998**, *51*, 783.

(12) Le Bail, P.; Bizot, H.; Ollivon, M.; Keller, G.; Bourgaux, C.; Buleon, A. *Biopolymers* **1999**, *50*, 99.

(13) Mori, K.; Uematsu, T.; Watanabe, H.; Yanagi, K.; Minobe, M. *Tetrahedron Lett.* **1984**, *25*, 3875.

(14) *Sybyl*, version 6.4; Tripos Associates. Inc.: St. Louis, MO, 1997.

(15) Rodriguez-Carvajal, J.; Roisnel, T. *FullProf.98* and *WinPLOTR*; New Windows 95/NT Applications for Diffraction; Newsletter No. 20; May−August, 1998.

(16) Mentzafos, D.; Mavridis, I. M.; Le Bas, G.; Tsoucaris, G. *Acta Crystallogr., Sect. B* **1991**, *47*, 746.

(17) Nyburg, S.; Faerman, C. H. *Acta Crystallogr., Sect. B* **1985**, *41*, 274.

(18) Szejtli, J. *Cyclodextrins and Their Inclusion Complexes*; Akademiai Kiado: Budapest, 1982.

(19) Tian, S. J.; Xi, G. X.; Cheng, Q. T.; Lou, X. D.; Li, J. H. *J. Therm. Anal*. **1998**, *53*, 825.